

# Hybrid films of polyimide containing in situ generated silver or palladium nanoparticles: Effect of the particle precursor and of the processing conditions on the morphology and the gas permeability

J. Compton<sup>a</sup>, D. Thompson<sup>a</sup>, D. Kranbuehl<sup>a</sup>, S. Ohl<sup>b</sup>, O. Gain<sup>b</sup>, L. David<sup>b</sup>, E. Espuche<sup>b,\*</sup>

<sup>a</sup> *Departments of Chemistry and Applied Science, College of William and Mary, Williamsburg, VA 23187, USA*

<sup>b</sup> *Ingénierie des Matériaux Polymères, IMP, UMR CNRS 5627, Laboratoire des Matériaux Polymères et des Biomatériaux, Université Claude Bernard-Lyon I, 69622 Villeurbanne Cedex, France*

Received 8 February 2006; received in revised form 20 April 2006; accepted 13 May 2006

Available online 12 June 2006

## Abstract

Hybrid organic/inorganic films have been prepared using different complexes soluble in a (BTDA/4,4'-ODA) poly(amic acid) solution. A silver based complex and two palladium based complexes were used and the metallic nanoparticles were formed by a single step process during the cure cycle applied to the film. Depending on the complex or the curing conditions used, either the nanoparticles formed were uniformly dispersed in the nanocomposite films, or the particles were also located at the film surface. The presence of the nanoparticles, whatever their composition, led to a decrease of the thermal degradation temperature in air atmosphere. The presence of 15 wt% of crystalline silver particles did not induce significant variation of the glass transition temperature and of the gas transport properties demonstrating low nanoparticle/matrix interactions. On the contrary, a pronounced effect in reducing the gas permeability for a wide variety of gases was observed for the nanocomposites containing the palladium based nanoparticles and this even for low palladium amount (5 wt%). Specific interactions between hydrogen and the Pd based nanoparticles were evidenced and the gas transport properties were discussed as a function of following parameters: the gas nature, the nanoparticle structure and composition, the developed morphology and the particle/matrix interactions.

© 2006 Elsevier Ltd. All rights reserved.

**Keywords:** Nanocomposites; Polyimide; Metal nanoparticles

## 1. Introduction

Organic–inorganic hybrid materials have attracted great attention because of their potential to combine the features of organic materials with those of inorganic materials. Particularly, organic–metal or metal oxide hybrid materials are promising functional materials in domains such as optical, electronic, magnetic, catalytic and gas transport applications. Two main methods can be used to prepare these materials: dispersion of preformed inorganic fillers [1,2] and in situ generation of inorganic fillers [3–14]. This second approach has become predominant these last years. In addition to the classical sol–gel method [3,4], different routes have been proposed, depending on the nanoparticle precursors, to obtain

inorganic clusters with tailored size, controlled size distribution and uniformly dispersed in the polymer matrix [5–10].

Palladium and silver nanoparticles have been obtained by Tröger et al. using a two step formation process [5]. The method consists in adding the metal precursor to a polymer solution and after complete mixing, in casting the solution to a film. The nanoparticles are then formed by a final and fast reduction step, after the solvent evaporation, using a methanol–sodium borohydride solution. This process is fast in comparison to reduction in diluted solutions of metal precursors [8,9], and according to the authors, it allows one to enlarge the choice of the polymer used as the nanocomposite matrix. Nevertheless, it still remains a two step process.

Recently, an in situ and single-step route to create a uniform dispersion of nanometer-sized metal or metal oxide clusters in polyimide matrices has been developed [11]. The process consists in thermally evolving from the dispersed complex in the polymer solution to a homogeneous dispersion of nanoparticles within the polymer matrix. In that case, the thermal treatment enables an internal metal ion reduction without the use and addition of external reducing agents.

\* Corresponding author. Tel.: +33 4 72 43 10 02; fax: +33 4 72 43 12 49.  
E-mail address: [eliane.espuche@univ-lyon1.fr](mailto:eliane.espuche@univ-lyon1.fr) (E. Espuche).

A uniform dispersion of nanometer-sized oxo-lanthanide (III) clusters (lanthanum, gadolinium, and holmium) in polyimide matrices has been achieved by this method and the nanocomposites based on  $\text{La}_2\text{O}_3$  nanoparticles have shown particularly strong matrix/particle interactions leading to enhanced gas barrier properties [12]. This single step method has also been applied to different silver complexes and in that case, reflective and electrically conductive surface silvered polyimide films have even been obtained [13,14]. It appears thus that different morphologies, and as a consequence different properties, can be achieved by this single step route depending on the nature of the metal complex and on the curing conditions.

The aim of this work is to study the influence of these parameters on the nanostructuration process and the final properties of systems based on the same polyimide matrix but on different metal complexes, a silver complex and two palladium complexes. The influence of the curing conditions has been studied for the system based on the silver complex and the effect of the ligand has been studied on palladium based systems. In both cases, particular attention has been paid to the developed morphology and the resulting properties, especially gas transport properties. Indeed, we have shown for the nanocomposites based on  $\text{La}_2\text{O}_3$  nanoparticles that these properties could be very sensitive to the interface developed between the particles and the matrix and bring, as a consequence, interesting information about the polymer/nanoparticle interactions [12]. Of particular interest, polyimides are characterized by specific gas permeability and selectivity properties and hydrogen is known to reduce oxidized palladium and to be soluble in metallic palladium clusters. It seems then to be very interesting to determine the gas transport mechanisms in systems composed of palladium-based nanoparticles imbedded in a polyimide matrix and to compare the properties of the nanocomposite membranes obtained by this single step process with those prepared by Tröger et al. using a two step formation process [5].

## 2. Experimental

### 2.1. Materials

The metal complexes used in this study are presented in Table 1. The (1,1,1-trifluoro-2,4-pentanedionato)silver (I), the bis(dimethyl sulfide)dichloropalladium, the bis(dimethyl-sulfide)dibromopalladium were created in situ using palladium (II) bromide, palladium (II) chloride, silver (I) acetate, dimethyl-sulfide, and 1,1,1-trifluoro-2,4-pentanedionate in the method described in Section 2.2. 3,3',4,4'-Benzophenone tetracarboxylic dianhydride (BTDA) and 4,4'-diaminodiphenylether (4,4'-ODA) were purchased from Chriskev Company, Inc. The BTDA was vacuum dried at 150 °C for 10 h and the 4,4'-ODA was used as received. Palladium (II) bromide and palladium (II) chloride were used as received from Pfaltz Bauer Inc. Silver (I) acetate, dimethylsulfide, and 1,1,1-trifluoro-2,4-pentanedionate were used as received from Aldrich Chemical.

### 2.2. Preparation of the nanocomposite films

Metal doped BTDA/4,4'-ODA poly(amic acid) solutions were prepared by first dissolving the metal complex in dimethylacetamide (DMAC), and then adding a DMAC solution of the poly(amic acid) to give a 15 wt% polymer (excluding the complex) solution. The polymer to complex mole ratio was calculated in order to obtain a theoretical weight percent of Pd and Ag in the final polyimide film equal to 5.2 and 13%, respectively, representing volume percents of 0.6 and 1.9%, respectively. These values were calculated on the basis of only silver (0), palladium (0) and polyimide remaining in the cured films. Ligands and ligand fragments were assumed to be volatilised from the film during the cure cycle. The metal precursor was first dissolved in the common solvent for both systems. Palladium chloride or bromide or silver acetate, respectively, were stirred for an hour until completely slurried. Then, 4 molequiv. of dimethylsulfide were added to the palladium halide solution whereas 1.35 molequiv. of 1,1,1-trifluoro-2,4-pentanedionate were added to the silver solution. The solutions were vigorously stirred during 2–4 h to obtain a homogeneous solution. The clear complex-doped resins were cast as films onto soda lime glass plates using a doctor blade set to give cured films ca. 40  $\mu\text{m}$  in thickness. After remaining in an atmosphere of slowly flowing dry air for 12–18 h, the films were cured according to the following conditions: heating over 20 min to 135 °C and holding for 1 h, heating to 300 °C over 4 h and holding at 300 °C for 1 h for the Pd films. For silver based films, the final curing step was either 1 h at 300 °C or 5 h at 300 °C. Thermal curing of the complex/(polyamic acid) film effects reduction of silver (I) and Pd (II) and metal particle formation coupled with cycloimidization of the amic acid. After a slow cooling to room temperature, the films were removed from the plate by soaking in warm deionized water, dried, and kept under atmospheric conditions until measurements were performed.

The nanocomposite films obtained with the silver complex were named (BTDA/4,4'-ODA)/Ag-300 °C 1 h and (BTDA/4,4'-ODA)/Ag-300 °C 5 h. The nanocomposite films obtained with the palladium bromide and the palladium chloride based complexes were named (BTDA/4,4'-ODA)/Pd-Br<sub>2</sub> and (BTDA/4,4'-ODA)/Pd-Cl<sub>2</sub>, respectively.

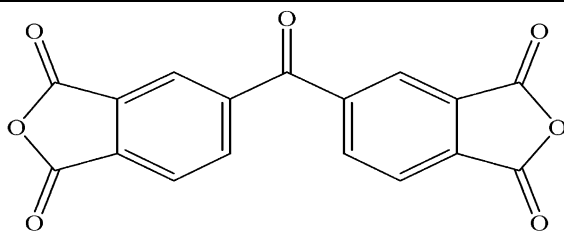
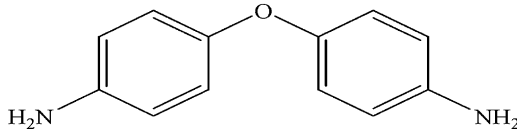
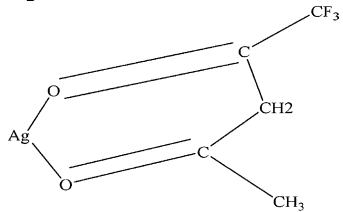
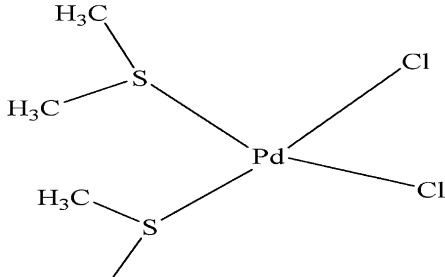
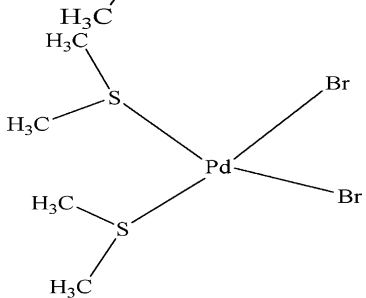
### 2.3. Characterization of the nanocomposite films

#### 2.3.1. Morphological and structural characterization of the nanoparticles

The morphology of the nanocomposite films was observed in SAXS experiments performed at the European Synchrotron Radiation facility (Grenoble-France) on BM2-D2AM beamline. A CCD camera was used (Ropper Scientific) and scattering diagrams were obtained after radial averages around the image center (location of the center of the incident beam). The data were collected in about 200 s, at an incident photon energy of 16 keV, and using silver behenate as a  $q$ -range calibration standard. The contribution of empty cell was subtracted by monitoring the transmitted intensity by means of

Table 1

Presentation of the different components used to synthesise the neat matrix and the nanocomposites

Name	Structure
BTDA 3,3',4,4'-benzophenone tetracarboxylic dianhydride	
4,4' ODA 4,4'-diaminodiphenylether	
(1,1,1-Trifluoro-2,4-pentanedionato)silver (I)	
Bis(dimethyl sulfide)dichloropalladium	
Bis(dimethyl sulfide)dibromopalladium	

a 8  $\mu\text{m}$  Kapton foil tilted at  $45^\circ$  and a photomultiplier in the first part of the evacuated tube.

TEM measurements were also performed in order to observe the nanoparticle dispersion. For TEM analysis, samples were microtomed at ambient temperature with a Leica EMFCS instrument equipped with a diamond knife in order to obtain ultrathin sections of about 80 nm thickness. Indeed, due to the high  $T_g$  values of the films it was not necessary to cut the samples at low temperature. The samples were imaged in a Philips CM120 transmission electron microscope with an accelerating voltage of 80 kV.

The nanoparticle crystalline structure was further studied by wide angle X-ray diffraction (WAXD) between  $5$  and  $90^\circ$  by step of  $0.02^\circ$  using a Cu tube and a Siemens D500

diffractometer, where the  $K\beta$  line was removed with a nickel filter. The films were deposited on neutral monosubstrates with a thin transfer adhesive with low scattering response.

### 2.3.2. Thermal properties

Differential scanning calorimetry (DSC) analysis was performed with a TA Instruments 2920 apparatus on samples of about 10 mg. Two scans ( $10^\circ\text{C}/\text{min}$ ) were successively recorded from  $35$  to  $300^\circ\text{C}$  with intermediate cooling ( $17^\circ\text{C}/\text{min}$ ).

Thermogravimetric analysis was performed with a TGA 2950 TA Instruments apparatus in air atmosphere and helium atmosphere. The samples (about 10 mg) were heated from  $30$  to  $800^\circ\text{C}$  at a heating rate equal to  $10^\circ\text{C}/\text{min}$ .

### 2.3.3. Gas transport mechanism analysis and background

The permeation cell used to carry out the gas permeation experiments consisted of two compartments separated by the studied membrane. Permeation measurements were performed at 20 °C. A preliminary high vacuum desorption was completed before each experiment. Gas permeation tests were carried out by feeding the single gases (purity level 99.998%) in the upstream compartment at a 3 bar pressure and by measuring the evolution of the pressure in the downstream compartment as a function of time with a 10 Torr datametrics pressure sensor.

The gas permeation in a pure polymer matrix is governed by a diffusion/solubility mechanism. The diffusion coefficient ( $D$ ) describes the kinetic aspect of the transport and the solubility coefficient ( $S$ ) reflects the penetrant/polymer matrix affinity and the thermodynamic aspect of the transport.

In a case of a Fickian transport, the permeability coefficient ( $P$ ) can be expressed by the following law:

$$P = DS \quad (1)$$

$P$  represents the volumetric gas flow rate going, in steady state conditions, through a defined membrane area submitted to a fixed pressure gradient and normalized on membrane thickness.

For ideal systems, the amount of gaseous molecules going through the membrane as a function of time can be determined by the integration of the Fick's second law. It can be represented by a curve in the transient state and by a straight line when steady-state conditions are attained [15].

The permeability coefficient can thus be determined from the slope of the linear dependence of the downstream pressure vs. time in the steady state and the diffusion coefficient can be deduced from the time lag,  $\theta$ , determined by the extrapolation of the steady state line on the time axis.

$$D = \frac{e^2}{6\theta} \quad (2)$$

where  $e$  is the film thickness.

Assuming a Fickian transport mechanism, the solubility coefficient  $S$  can be calculated as ratio between the permeability and diffusivity values according to Eq. (1).

The ideal permselectivity defined as the ratio between the permeability of two gases is thus equal to the product of the diffusion selectivity and the solubility selectivity.

For hybrid membranes, the gas transport mechanism can become more complex. Assuming in all cases that the continuous polymer phase keeps the same specific properties than the neat polymer, different cases can be considered depending on the filler/gas interactions and filler/matrix interface.

When poor polymer/particles interactions are developed in the hybrid systems, voids can be created at the matrix/filler interface leading to no improvement in the selectivities over the original polymer because of by pass of gas penetrants around the particles [16].

When the polymer/filler interface is strong enough, the fillers can induce different effects on the gas transport properties depending on their interactions towards the diffusing molecules:

(i) If the particles are impermeable to the gases, a decrease of solubility is expected for the nanocomposites due to a reduced polymer matrix volume (Eq. (3)) and a decrease in diffusion is expected due to a more tortuous path for diffusing molecules (Eq. (4)) [17]

$$S_c = S_m(1 - \phi_d) \quad (3)$$

$$D_c = \frac{D_m}{\tau} \quad (4)$$

where  $S_c$  and  $S_m$  are the solubility coefficients of the composite and the neat matrix, respectively,  $D_c$  and  $D_m$  are the diffusion coefficients of the composite and the neat matrix, respectively,  $\phi_d$  is the volume fraction of the impermeable dispersed phase and  $\tau$  the tortuosity.

As a consequence and assuming a Fickian transport mechanism, a gas permeability decrease is observed. It can be described by Maxwell law [18] for spherical impermeable dispersed particles or Nielsen law [17] (Eq. (5)).

$$P_c = \frac{2(1 - \phi_d)}{2 + \phi_d} P_m \quad (5)$$

where  $P_c$  and  $P_m$  are the permeability coefficients of the composite and the matrix, respectively. Indeed the tortuosity factor  $\tau$  is expressed in that case by:

$$\tau = 1 + \frac{\phi_d}{2} \quad (6)$$

In this approach, the relative decrease of all the transport parameters is independent of the penetrant nature and size and no change of the gas selectivity is observed compared to the neat matrix.

(ii) When specific interactions are developed between the particle and the diffusive molecule, different behaviors can be observed.

In some cases, especially for matrices containing molecular sieves, an increase of both selectivity and permeability can be observed and it is generally attributed to favorable adsorption kinetics [19].

For membranes containing 'active' fillers, the diffusion time lag is generally increased as consequence of immobilizing adsorption or a reaction. An additional time is required to accumulate the excess penetrant before steady-state can be reached [20,21]. In that case, the dispersed particles consume or trap the solute as it diffuses across the membrane. Eventually, enough solute will diffuse into the membrane to exhaust the active particles. Solute can then diffuse steadily across the membrane as it would across an initially unreactive film.

In this work, the gas transport in the neat polyimide matrix and in the hybrid organic/inorganic membranes has been studied according to these different cases for different gases (helium, carbon dioxide, oxygen and hydrogen). The three gas transport parameters have been determined.  $P$  was expressed in

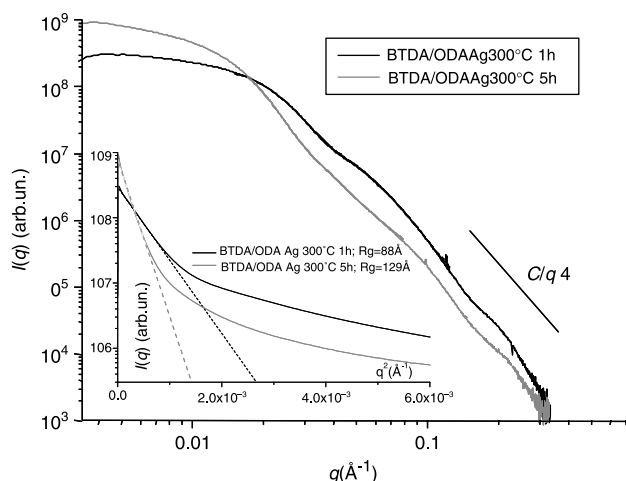


Fig. 1. SAXS patterns of BTDA/ODA Ag systems, showing the influence of the curing history. The size of the particles is deduced from the Guinier law  $I(q) = I_0 \exp(-R_g^2 q^2/3)$  in the low- $q$  range ( $q < 0.03 \text{ \AA}^{-1}$ ).

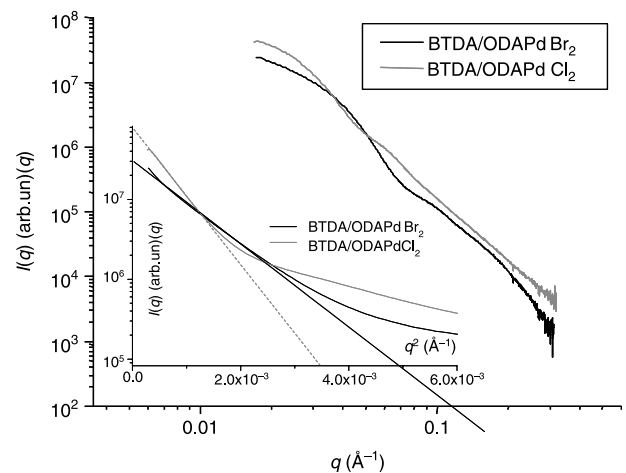


Fig. 2. SAXS patterns of BTDA/ODA Pd systems, showing the influence of the ligand type. The size of the particles is deduced from the Guinier law  $I(q) = I_0 \exp(-R_g^2 q^2/3)$  in the low- $q$  range ( $q < 0.03 \text{ \AA}^{-1}$ ).

Barrer with  $1 \text{ Barrer} = 10^{-10} \text{ cm}_{\text{STP}}^3 \text{ cm cm}^{-2} \text{ s}^{-1} \text{ cm}_{\text{Hg}}^{-1}$ .  $D$  was deduced from the time lag method and expressed in  $\text{cm}^2 \text{ s}^{-1}$ .  $S$  was calculated according to Eq. (1) and expressed in  $\text{cm}_{\text{STP}}^3 \text{ cm}^{-3} \text{ cm}_{\text{Hg}}^{-1}$ . The accuracy on the transport coefficients

was estimated to be less than  $\pm 5\%$ . It was not possible to determine with a good precision the diffusion coefficient for helium and as a consequence the helium solubility. Indeed the time lag was too small for this non interactive, very small gas.

### 3. Results and discussion

The morphology of the nanocomposite films has been studied as a function of the complex nature for the palladium based nanocomposites and as a function of the curing procedure for the silver based nanocomposites. Whatever the nanocomposite film, the scattering curves obtained by SAXS are representative of a diluted particulate system (Figs. 1 and 2) and the morphological analysis using the Guinier approach [22] allows the average gyration radius of the spherical particles ( $R_g$ ) to be determined. The values reported in Table 2 show that the particles are in the range of nanometer sized for all systems and that the silver based particles obtained after a final curing step of 5 h at 300 °C are the largest ones. At large  $q$ -values (i.e.  $q > 0.04 \text{ \AA}^{-1}$ ), several oscillations around the Porod's asymptote ( $I(q) \sim C/q^4$ ) can be observed for Ag based systems, as a result of the spherical shape and narrow size distribution of the particles (Fig. 1).

The TEM images of the different nanocomposite films bring additional information about the nanoparticle dispersion. The nanoparticles are uniformly distributed within the polymer when using the bromide palladium based complex (Fig. 3(a)). The discrete nanoparticle diameters are predominantly close to 10 nm thus in good agreement with the  $R_g$  values determined by SAXS. The characteristic inter-particle distances are much higher than the radius of the particles. This observed morphology is in agreement with the SAXS scattering curves and the frame of analysis of diluted systems.

A different morphology is achieved with the chloride palladium based complex. Nanoparticles with mean diameter of about 10 nm are still uniformly distributed within the polymer but in addition we can observe a surface layer of Pd of about 60 nm thick (Fig. 3(b)). This layer seems to be continuous at the observation scale we used.

As a result, the influence of the nature of the palladium complex ligand is clearly evidenced on the morphology that is nanoparticle dispersion. Different structures of the complex

Table 2

Thermal and morphological data for the neat polyimide film and the composite films: glass transition temperature of the films ( $T_g$ ), temperature at which the mass loss reaches 10% and morphological parameters determined by SAXS and TEM ( $R_g$ : gyration radius of the particles)

Systems	(BTDA/4,4'-ODA)	(BTDA/4,4'-ODA)/Pd-Cl <sub>2</sub>	(BTDA/4,4'-ODA)/Pd-Br <sub>2</sub>	(BTDA/4,4'-ODA)/Ag-300 °C 5 h	(BTDA/4,4'-ODA)/Ag-300 °C 1 h
$T_g$ (°C) first scan	272	a	a	271	272
$T_g$ (°C) second scan	273	a	a	270	268
TGA 10% wt loss in helium: $T_{10}$ (°C)	556	558	559	540	545
TGA 10% wt loss in air: $T_{10}$ (°C)	556	354	478	400	392
$R_g$ (nm) <sup>b</sup>	No particle	4.0	5.0	8.8	12.9
Diameter of the nanoparticles in bulk (nm) <sup>c</sup>	No particle	10	10	5–35	20

<sup>a</sup>  $T_g$  could not be determined.

<sup>b</sup> Determined by SAXS analysis.

<sup>c</sup> Determined by TEM analysis.

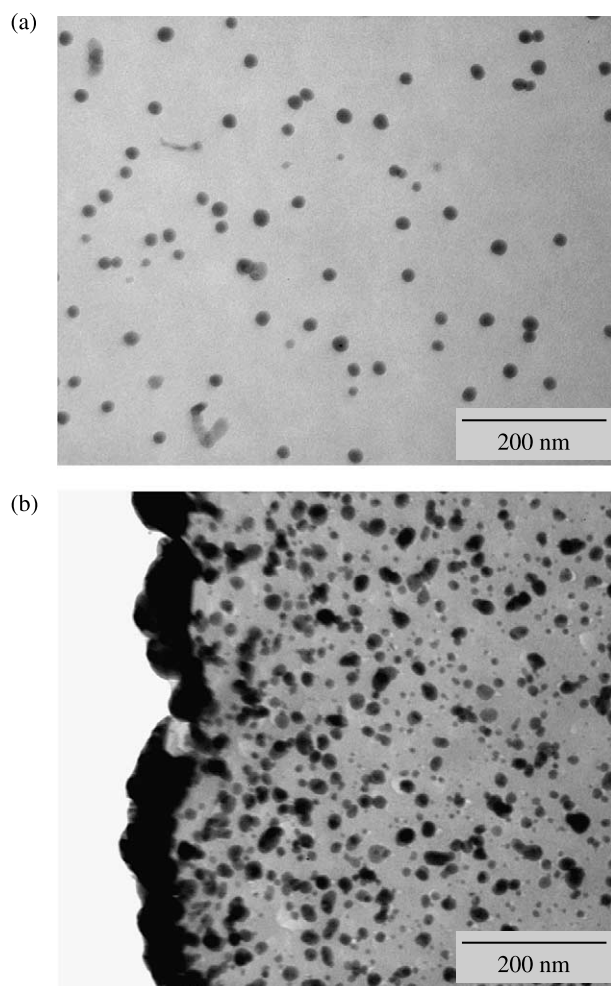


Fig. 3. TEM images of (a) (BTDA/4,4'-ODA)/Pd-Br<sub>2</sub> nanocomposite and (b) (BTDA/4,4'-ODA)/Pd-Cl<sub>2</sub> nanocomposite.

ligands can indeed lead to different matrix/metal complex interactions and as a consequence to different final morphologies. This phenomenon has already been underlined by several authors [5,13]. Tröger et al. [5] observed that their metal particles generation process using AgBF<sub>4</sub>, AgAc, PdAc<sub>2</sub> (where Ac corresponds to acetate) worked best with polymer containing amide bonds. Southward et al. [13] obtained very different morphologies using the same polymer matrix but two silver complexes differing only by one trifluoromethyl group. Thus, according to our results and the literature data, subtle changes in ligand structure can have pronounced effects on films properties.

Two different morphologies are also observed on silver based nanocomposites depending in that case on the curing time at 300 °C. The nanocomposite films cured for 1 h at 300 °C exhibit a uniform distribution of nanometer-sized metal particles within the film (Fig. 4(a)). It can be remarked that the size distribution of the silver based particles is larger than that observed for the palladium based particles. The particle diameters are indeed ranging from 5 to 35 nm. For a longer thermal treatment time at 300 °C, a layer of metal is formed at the film surface in addition to an homogeneous dispersion of

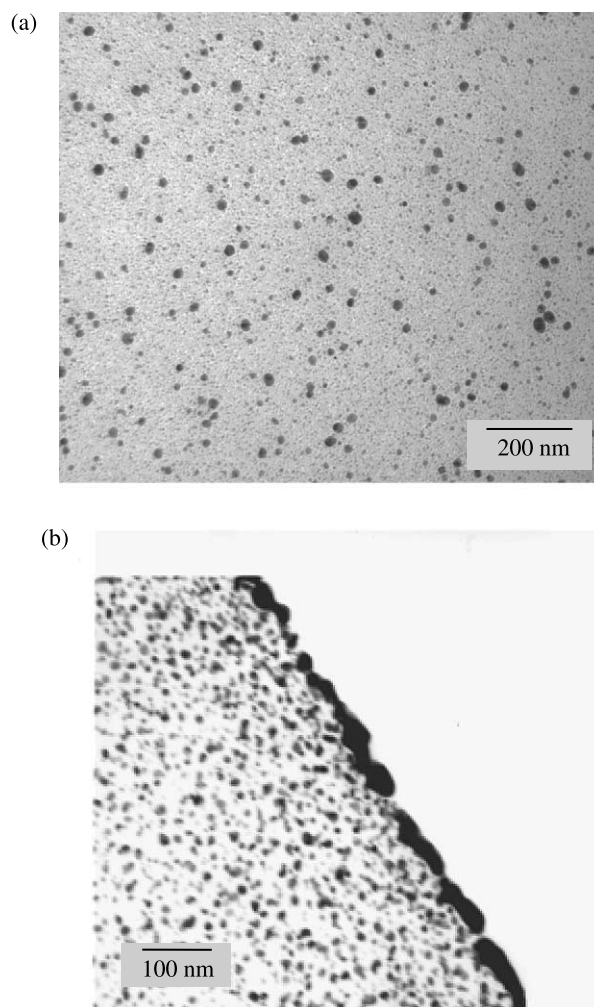


Fig. 4. TEM images of (a) (BTDA/4,4'-ODA)/Ag 300 °C 1 h nanocomposite and (b) (BTDA/4,4'-ODA)/Ag 300 °C 5 h nanocomposite.

nanosized particles within the films (Fig. 4(b)). This surface layer has the same thickness as that of Pd but it seems to be a non-continuous surface layer in this case. Furthermore, the size of the nanoparticles seems to increase as they are located near to the surface. This can explain why the average gyration radius determined by SAXS is higher for (BTDA/4,4'-ODA)/Ag-300 °C 5 h films.

Thus, the curing conditions represent a dominant factor for the silver nanocomposite morphology. It seems that a silver particle migration/aggregation is promoted as the curing time at 300 °C increases. Similar observations have been reported in the literature by Southward et al. [13]. These authors showed that it was possible to prepare silver/polyimide films with both exceptional reflectivity and conductivity. They analyzed the developed morphology and the film properties as a function of the curing conditions and concluded that a migration of silver particles occurred as a function of the curing time at 300 °C. According to the authors, the formation of a conductive film required, in addition to this migration process, a silver promoted surface oxidative degradation of polyimide to volatile products, which then forced nanometer size silver aggregates into contact.

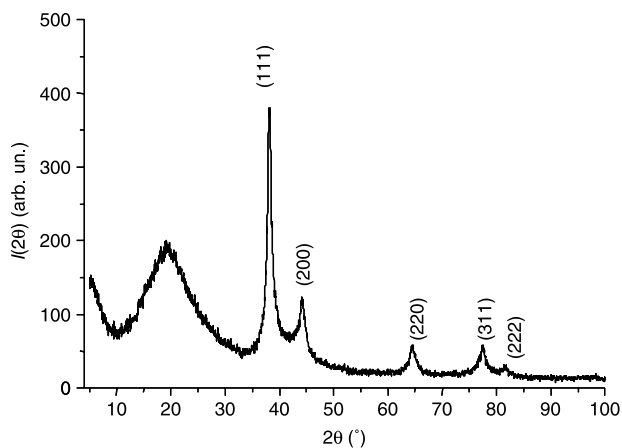


Fig. 5. Diffraction patterns in reflection mode of BTDA/ODA/Ag-300 °C 5 h. (13% Ag w/w).

It seems that according to our results and the literature data, both the complex ligand and the cure cycle applied to the systems are important parameters for the final nanoparticles dispersion. Furthermore, the degradation of the composite films has also to be considered to explain some specific properties. Before presenting the results relative to the degradation study of our systems under different atmospheres we will focus first on the structure and composition of the nanoparticles developed in the different systems.

The structure of the nanoparticles has been studied by WAXD. Whatever the curing atmosphere and time at 300 °C, we can observe the diffraction peaks of f.c.c. crystalline silver on the diffraction patterns of the silver-based nanocomposites (Fig. 5). A well defined amorphous halo is the contribution of the polyimide matrix.

The particles formed in the (BTDA/4,4'-ODA)/Pd-Cl<sub>2</sub> films are also crystalline as evidenced by the well defined diffraction peaks of f.c.c. metallic palladium (namely the 111, 200, 220, 311 and 222 diffraction peaks). The presence of palladium oxide PdO is suspected, since low intensity additional peaks could be noticed (on pattern (b) and (c) on Fig. 6) at diffraction angles that could correspond to PdO structure (namely the (100) line reported at  $2\theta = 29.76^\circ$ , (002) + (101) at  $34.47^\circ$ , and the (110) at  $42.58^\circ$ ).

The diffraction patterns of the (BTDA/4,4'-ODA)/Pd-Br<sub>2</sub> films do not show intense and well defined diffraction peaks contrary to the (BTDA/4,4'-ODA)/Pd-Cl<sub>2</sub> films. Nevertheless, the presence of crystalline palladium and of PdO structures cannot be excluded (a diffraction line close to  $2\theta = 29.8^\circ$  is again indicative of the (100) PdO reflection (pattern (a) on Fig. 6) and the low amount of Pd and PdO in addition to broadened reflections could explain the absence of other well defined diffraction peaks).

DSC analysis was used to determine the glass transition temperature of the different nanocomposites and neat polyimide films (Table 2). No great differences in  $T_g$  values are observed between the neat reference and the silver based nanocomposites containing 13 wt% of silver (Fig. 7(a)). According to these results, it seems that little to no variation

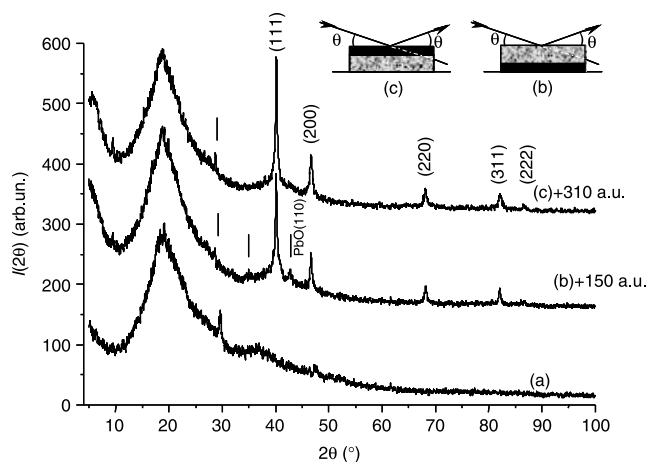


Fig. 6. Diffraction patterns in reflection mode of (a) BTDA/ODA/Pd-Br<sub>2</sub> with 5% Pd w/w; (b) BTDA/ODA/Pd-Cl<sub>2</sub> with reversed metallic surface (5% Pd w/w) (c) BTDA/ODA/Pd-Cl<sub>2</sub> with (5% Pd w/w) and metallic surface on X-ray side (the inserts display schematically the orientation of the samples during the (b) and (c) WAXS experiment). The curves (b) and (c) have been shifted for clarity.

in chain mobility near the nanoparticle's surface is observed or that this variation could not be evidenced by classical DSC analysis. It was not possible to detect a variation in the change in heat capacity,  $\Delta C_p$ , and as a consequence to determine the glass transition temperature for the two palladium based systems (Fig. 7(b)). Nevertheless the palladium content was low in that case (5 wt%) and the experimental conditions used for  $T_g$  determination were exactly the same as for silver based nanocomposites. As a result, the palladium nanoparticles seem to have a higher effect on the polymer matrix than the silver

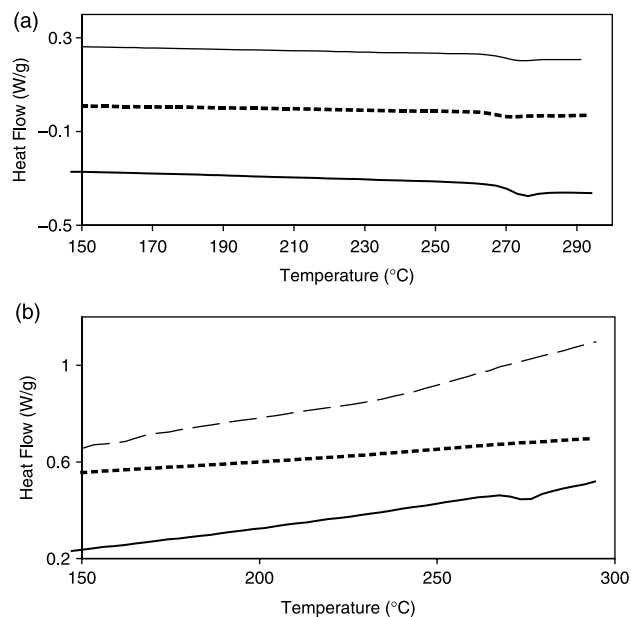


Fig. 7. (a) DSC thermograms of (—) neat polyimide film, of (---) (BTDA/4,4'ODA)/Ag 300 °C 1 h and of (—) BTDA/ODA/Ag 300 °C 5 h. (b) DSC thermograms of (—) neat polyimide film, of (---) (BTDA/ODA)/Pd-Br<sub>2</sub> and of (---) (BTDA/ODA)/Pd-Cl<sub>2</sub>.

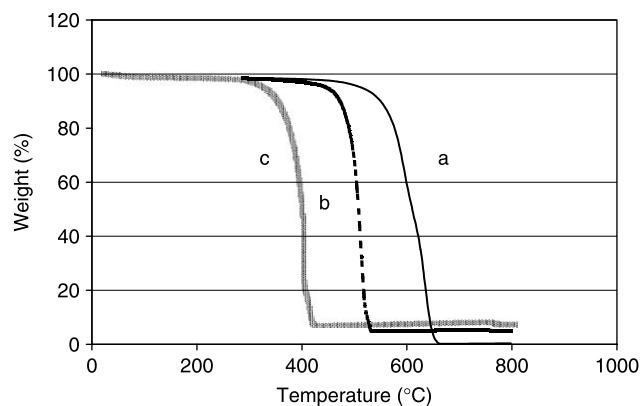


Fig. 8. Evolution of the weight as a function of the temperature determined by thermogravimetric analysis on (a) the neat polyimide (b) (BTDA/4,4'-ODA)/Pd-Br<sub>2</sub> nanocomposite and (c) (BTDA/4,4'-ODA)/Pd-Cl<sub>2</sub> nanocomposite.

nanoparticles have and further study is under progress to analyze in these systems the chain mobility in presence of fillers using thermomechanical analysis.

The thermal degradation of the different materials has been studied in different atmospheres, helium and air. The mass loss curves obtained in air are plotted in Figs. 8 and 9 for palladium based systems and silver based systems, respectively. The values of the temperature at which the mass loss reaches 10%,  $T_{10}$ , are reported in Table 2. No great variation of  $T_{10}$  values are observed when TGA analysis are performed in helium atmosphere. On the other hand, the thermal degradation curves determined in air show a significant decrease of the thermal stability of the nanocomposites compared to the parent film whatever the nanoparticle composition (Figs. 8 and 9). Thus, it appears that palladium and silver metals catalyze oxidative degradation. It can be observed that the temperature at which thermal degradation begins is lower for (BTDA/4,4'-ODA)/Pd-Cl<sub>2</sub> than for (BTDA/4,4'-ODA)/Pd-Br<sub>2</sub> (Fig. 8) showing in that case also the importance of the complex ligand on the final nanocomposite properties. The curves relative to the silver based nanocomposites obtained with the two different curing

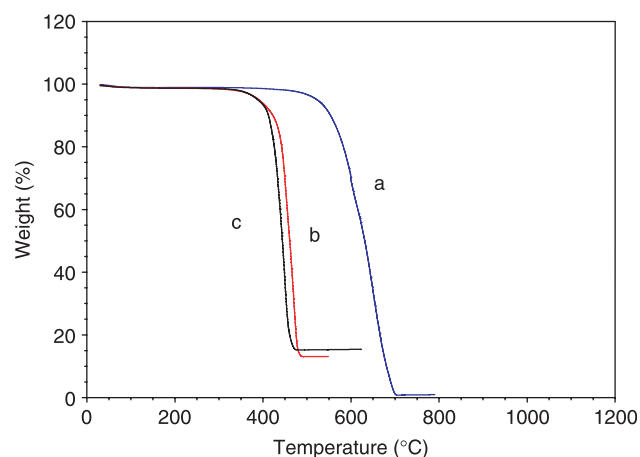


Fig. 9. Evolution of the weight as a function of the temperature determined by thermogravimetric analysis on (a) the neat polyimide (b) (BTDA/4,4'-ODA)/Ag 300 °C 1 h nanocomposite and (c) (BTDA/4,4'-ODA)/Ag 300 °C 5 h nanocomposite.

conditions are on the other hand very similar (Fig. 9) and the value of the temperature corresponding to a weight loss of 10% remains near to 400 °C. For all the studied systems, the weight percentages measured at the final plateau correspond quite well to the theoretical metal contents calculated presuming that all ligands and ligand fragments of the complex are volatilised from the film during the cure cycle.

The gas transport coefficients determined on the films stored under atmospheric conditions are reported in Table 3. For the nanocomposites with a surface metal layer, the 'metallized' face was always placed in the upstream side of the permeation cell in order to perform the gas permeation experiments.

The permeability and diffusion coefficients measured on the neat BTDA/4,4'-ODA polyimide are in good agreement with those reported in the literature and they underline the low permeability of the neat films [23].

The presence of silver nanoparticles in the films does not lead to significant variation of the gas transport properties despite the relatively high content of silver (13 wt%). This result is not in agreement with the behavior generally observed for membranes comprising inorganic fillers and with the variation reported by Tröger et al. [5] who observed for an equivalent silver metal loading (15 wt%) a decrease of both permeability and diffusion coefficients for nitrogen and hydrogen. The differences observed in gas transport results cannot be explained by a difference in the size and composition of the particles obtained by the two types of process. We suggest that this is most likely explained by an interface effect: a weak interface seems to be developed between the silver particles and the polyimide matrix in our systems. This lack of strong interactions between the particles and the matrix could also explain the particle migration/aggregation phenomenon observed as a function of the curing time at 300 °C and the invariance of the glass transition temperature compared to the parent film.

For palladium based nanocomposites, the gas transport results are discussed as a function of the gas nature and of the gas/particle interaction. The gas permeability measurements have been made in the following order: He, CO<sub>2</sub>, O<sub>2</sub> and H<sub>2</sub>.

### 3.1. He, CO<sub>2</sub> and O<sub>2</sub> transport mechanisms

A decrease of the He, CO<sub>2</sub>, and O<sub>2</sub> permeability coefficients is observed for (BTDA/4,4'-ODA)/Pd-Br<sub>2</sub> nanocomposite film compared to the neat matrix. The relative permeability, the permeability of the nanocomposite ratioed to the permeability of the neat matrix is similar for these three gases despite their very different sizes. No great variation of the CO<sub>2</sub> and O<sub>2</sub> solubility is noticed and a significant CO<sub>2</sub> and O<sub>2</sub> diffusion rate decrease is observed. All these observations show that the palladium nanoparticles act as a diffusion barrier for these gases. Indeed the theoretical palladium volume fraction is low (less than 1%) explaining the invariance of the solubility coefficient. At this low volume %, the homogeneous dispersion of the nanometer sized particles in the polymer matrix leads to an important tortuosity effect and, as a consequence, to a decrease of both diffusion and permeability coefficients.



Table 3  
Permeability ( $P$ ), diffusion ( $D$ ) and solubility ( $S$ ) coefficients determined for different gases on the films stored under atmospheric conditions

Systems	(BTDA/4,4'-ODA)	(BTDA/4,4'-ODA)/Pd-Cl <sub>2</sub>	(BTDA/4,4'-ODA)/Pd-Br <sub>2</sub>	(BTDA/4,4'-ODA)/Ag-300 °C 5 h	(BTDA/4,4'-ODA)/Ag-300 °C 1 h
$P$ He	4.48	2.77	2.93	–	–
$P$ CO <sub>2</sub>	0.56	0.26	0.365	0.689	0.62
$D$ CO <sub>2</sub> ( $\times 10^{10}$ )	4.72	2.5	3.15	4.61	4.46
$S$ CO <sub>2</sub> ( $\times 10^1$ )	1.21	1.04	1.12	1.49	1.39
$P$ O <sub>2</sub>	0.15	0.071	0.107	0.166	0.16
$D$ O <sub>2</sub> ( $\times 10^9$ )	2.27	1.25	1.80	1.97	2.5
$S$ O <sub>2</sub> ( $\times 10^3$ )	6.6	5.7	5.94	8.46	7.2
$P$ H <sub>2</sub>	3.51	1.77	2.08	3.59	3.53
$D$ H <sub>2</sub> ( $\times 10^7$ )	15.4	0.0408	2.38	16	15.9
$S$ H <sub>2</sub> ( $\times 10^4$ ) <sup>b</sup>	2.28	434	8.74	2.24	2.22

$P$  is expressed in Barrer units,  $D$  in  $\text{cm}^2 \text{s}^{-1}$ ,  $S$  in  $\text{cm}^3 \text{cm}^{-3} \text{cmHg}^{-1}$ .

The experimental permeability decrease by about 35% is much higher than the theoretical decrease calculated by Maxwell law [18] (less than 1%) underlining, as for La<sub>2</sub>O<sub>3</sub>, a nanocomposite effect and the formation of a strong interface between the particles and the matrix [12].

Improved gas barrier properties are even observed for the (BTDA/4,4'-ODA)/Pd-Cl<sub>2</sub> nanocomposite. The gas permeability is reduced in that case by a factor 2 compared to the neat matrix. This result can be related to the formation of a surface layer of crystalline palladium based particles. Nevertheless it can be remarked that this layer is not totally impermeable to gases.

### 3.2. H<sub>2</sub> transport mechanism

The decrease of the H<sub>2</sub> permeability is similar to that measured for He, CO<sub>2</sub> and O<sub>2</sub>. We observe for this gas an important increase of the time lag corresponding to a high decrease of the apparent gas diffusion rate. Indeed, compared to the neat matrix, DH<sub>2</sub> is divided by a factor 6.5 for (BTDA/4,4'-ODA)/Pd-Br<sub>2</sub> nanocomposite and by a factor 377 for (BTDA/4,4'-ODA)/Pd-Cl<sub>2</sub>. We can thus conclude that H<sub>2</sub> gas transport mechanism is for these materials very different from He transport mechanism despite the very similar size of these two gaseous molecules [24]. This difference can be explained by specific H<sub>2</sub>/palladium based nanoparticle interactions that are confirmed by the high value of the H<sub>2</sub> solubility deduced from the permeability and diffusion coefficients according to Eq. (1). Indeed compared to the neat matrix, the H<sub>2</sub> solubility

coefficient increases by a factor of 3.8 for (BTDA/4,4'-ODA)/Pd-Br<sub>2</sub> and by a factor of 190 for (BTDA/4,4'-ODA)/Pd-Cl<sub>2</sub>.

A two step gas transport mechanism can be proposed to explain the variation of the three H<sub>2</sub> transport parameters. During the first step, H<sub>2</sub> diffuses through the polymer by normal Fickian process but upon encounter with the palladium based nanospheres it is trapped or consumed. As a consequence the steady state is delayed. It can only be established after the concentration of H<sub>2</sub> trapped or consumed molecules equals the maximum interaction/reaction capacity of the particles. When this second step is reached, H<sub>2</sub> diffusion is apparently that of an inactive gas and palladium nanoparticles only induce a tortuosity effect. Thus, the gas flux decrease in steady state is similar to that observed for other gases. This kind of behaviour has been already observed towards CO<sub>2</sub> with some zeolites dispersed in a polymer matrix [25] and towards H<sub>2</sub> for other palladium based nanocomposites [5]. One consequence of this two step transport mechanism is that, compared to the neat matrix, the nanocomposites H<sub>2</sub>/gas permeability selectivity is unchanged whereas the H<sub>2</sub>/gas solubility selectivity increases and the H<sub>2</sub>/gas diffusion selectivity decreases.

As previously mentioned, two possible mechanisms can explain the H<sub>2</sub> first step transport: a dissolution mechanism in palladium clusters leading to a high solubility value or a reduction reaction that consumes H<sub>2</sub> molecules. This last mechanism assumes the presence of palladium oxide. As PdO structure has been suspected from WAXD analysis for all the palladium based nanocomposites, we have performed a new series of gas transport experiments in order to study the redox

Table 4  
Redox behaviour of the (BTDA/4,4'-ODA)/Pd-Cl<sub>2</sub> nanocomposite: evolution of the hydrogen and oxygen transport coefficients on the same nanocomposite film exposed to successive permeation experiments

Permeation experiment	First H <sub>2</sub> permeation experiment	Second H <sub>2</sub> permeation experiment	Third H <sub>2</sub> permeation experiment	First O <sub>2</sub> permeation experiment
$P$ H <sub>2</sub> (Barrer)	1.8	1.84	1.84	–
$D$ H <sub>2</sub> ( $10^{-7} \text{cm}^2 \text{s}^{-1}$ )	0.0365	0.357	0.28	–
$S$ H <sub>2</sub> ( $10^{-4} \text{cm}^3 \text{cm}^{-3} \text{cmHg}^{-1}$ )	493	51	66	–
$P$ O <sub>2</sub> (Barrer)	–	–	–	0.075
$D$ O <sub>2</sub> ( $10^{-9} \text{cm}^2 \text{s}^{-1}$ )	–	–	–	0.49
$S$ O <sub>2</sub> ( $10^{-3} \text{cm}^3 \text{cm}^{-3} \text{cmHg}^{-1}$ )	–	–	–	15.3

behaviour of the nanocomposites. These experiments were performed on the (BTDA/4,4'-ODA)/Pd-Cl<sub>2</sub> nanocomposite. At first, a H<sub>2</sub> permeation experiment was performed on a nanocomposite film followed by a desorption under secondary vacuum during 1 h. It was verified that this desorption step was long enough to take off from the films all the reversibly sorbed gases. This protocol was repeated three fold and then one O<sub>2</sub> permeation experiment was performed.

The results are presented in Table 4. We can see that the H<sub>2</sub> permeability coefficient is similar for the three H<sub>2</sub> permeation experiments. On the contrary, an increase of the apparent H<sub>2</sub> diffusion coefficient by two orders of magnitude is observed between the first and the second experiment and then the apparent H<sub>2</sub> diffusion coefficient seems to reach a constant value. As a consequence the apparent H<sub>2</sub> solubility coefficient decreases by two orders of magnitude between the first and the second experiment and it then seems to reach a constant value. The O<sub>2</sub> permeability measured after this series of experiments is similar to that measured on membranes conditioned under air but we can observe a large decrease of the apparent O<sub>2</sub> diffusion rate and an increase of the O<sub>2</sub> solubility.

Regarding the evolution of the apparent H<sub>2</sub> diffusivity and solubility let us presume that during the first permeation experiment, a large fraction of the H<sub>2</sub> molecules that encounter the particles react with palladium oxide or are strongly chemisorbed. The reaction and chemisorption in the first step result in more H<sub>2</sub> molecules passing through in the second step. That is why the apparent H<sub>2</sub> diffusion coefficient increases in the second H<sub>2</sub> permeation experiment leading to a decrease of the apparent H<sub>2</sub> solubility. As the H<sub>2</sub> molecules sorbed in this second experiment are not tightly bonded to the nanoparticles, this second sorption phenomenon is totally reversible and the third experiment leads to equivalent H<sub>2</sub> diffusion and solubility values. Concerning the O<sub>2</sub> transport mechanism performed on these H<sub>2</sub> pre-treated membranes, the decrease of the O<sub>2</sub> apparent diffusivity and the increase of the O<sub>2</sub> solubility compared to the values measured on air-stored membranes reflect the oxidation of the clusters in the membrane or possible reactions with the highly chemisorbed H<sub>2</sub> molecules in the clusters. Further work is in progress now in order to determine the contribution of each mechanism.

From a general point of view, all the gas transport mechanisms evidenced on our palladium based polyimide nanocomposites are consistent with the results obtained by Tröger et al. [5] on nanocomposites based on a poly(amide-imide) matrix and palladium based nanoparticles. In the Tröger study [5], the nanoparticles were composed of metallic palladium and PdO structures and all the particles were homogeneously dispersed in the films. The evolution of the gas transport properties reported by Tröger with 15 wt% palladium are comprised between those we have observed with the bromide palladium complex and the chloride palladium complex at 5 wt% of palladium. These results clearly underline the interest of obtaining crystalline palladium particles and a specific location of the nanoparticles, that is the formation of a palladium based surface layer.

#### 4. Conclusion

Hybrid organic/inorganic films have been prepared by a single step process using different complexes (a silver based complex and two palladium based complexes) soluble in a BTDA/4,4'-ODA polyimide solution. Nanocomposites have been obtained in all cases but different morphologies, that is, nanosphere dispersion, matrix/particle interactions and properties have been achieved as a function of the particle precursor and of the processing conditions.

For silver based nanocomposites, it has been shown that a uniform dispersion of nanometer sized spheres could be obtained during the thermal curing applied to the initial homogeneous (silver complex/polyimide) solution. The nanoparticles composition was clearly identified as f.c.c. crystalline silver. Increasing the time held at the final curing step (300 °C) led to a silver migration/aggregation phenomenon and to a more complex morphology. Indeed, in addition to a homogeneous dispersion of very small nanospheres, larger nanoparticles were formed near to the surface and silver 'islands' were observed at the film surface. The formation of weak nanoparticle/matrix interactions was suspected to be at the origin of this morphological evolution. The small variation of the glass transition temperature and of the gas transport properties of the nanocomposite films compared to the parent films reinforced this hypothesis.

For palladium based nanocomposite a large effect of the complex ligand was underlined on the nanoparticle dispersion. The nanoparticles developed for the bromide palladium complex were homogeneously dispersed in the bulk of the matrix. The morphology was much more complex with the chloride palladium based complex since it consisted of a palladium surface layer in addition to a homogeneous dispersion of nanoparticles in the bulk. The nanoparticles were constituted of f.c.c. crystalline palladium and of PdO structures. Independently of their chemical composition, the nanoparticles had a pronounced effect in reducing the gas permeability underlining strong particle/matrix interactions and an important tortuosity effect. The presence of a metallised surface increased the barrier effect. Specific interactions between hydrogen and the Pd based nanoparticles were evidenced and explained by a chemisorption of H<sub>2</sub> molecules in the crystalline Pd structures and a reduction of PdO.

It was thus shown that it is possible to obtain, by this method and the appropriate choice of the complex and of the curing conditions, nanocomposites with modulated specific properties.

#### Acknowledgements

D.W. Thompson expresses thanks to the Jeffress Memorial Trust for partial support of this work.

#### References

- [1] Radheshkumar C, Münstedt H. *Mater Lett* 2005;59:1949–53.
- [2] Delmonte J. *Metal/polymer composites*. New York: Van Nostrand Reinhold; 1990.

- [3] Zoppi RA, Das Neves S, Nunes SP. *Polymer* 2000;41:5461–70.
- [4] Lu Z, Liu G, Duncan S. *J Membr Sci* 2003;221:113–22.
- [5] Tröger L, Hinnefeld H, Nunes S, Oehring M, Fritsch D. *J Phys Chem B* 1997;101:1279–91.
- [6] McKeown NB, Budd PM, Msayib KJ, Ghanem BS, Kingston HJ, Tattershall CE, et al. *Chem Eur J* 2005;11:2610–20.
- [7] Porel S, Singh S, Harsha SS, Rao DN, Radhakrishnan TP. *Chem Mater* 2005;17:9–12.
- [8] Bradley JS, Hill EW, Behal S, Klein C. *Chem Mater* 1992;4:1234.
- [9] Toshima N, Harada M, Yonezawa T, Kushihashi K, Asakura KJ. *Phys Chem* 1991;95:7448.
- [10] Gubin SP. *Colloids Surf* 2002;202:155–63.
- [11] Thompson DT, Thompson DW, Southward RE. *Chem Mater* 2002;14:30–7.
- [12] Espuche E, David L, Rochas C, Afeld JL, Compton JM, Thompson DW, et al. *Polymer* 2005;46(17):6657–65.
- [13] Southward RE, Stoakley DM. *Prog Org Coat* 2001;41:99–119.
- [14] Warner JD, Pevzner M, Dean CJ, Kranbuehl DE, Scott JL, Broadwater ST, et al. *J Mater Chem* 2003;13:1847–52.
- [15] Petropoulos JH. Mechanism and theories for sorption and diffusion of gases in polymers. In: Paul DR, Yampolskii YP, editors. *Polymeric gas separation membranes*. Boca-Raton: CRC Press; 1994. p. 17–82.
- [16] Vankelecom IFJ, Merckx E, Luts M, Uytterhoeven JB. *J Phys Chem* 1995;99:13187–92.
- [17] Nielsen LE. *J Macromol Sci* 1967;A1:929.
- [18] Barrer RM. Diffusion in polymers. In: Crank J, Park GS, editors. *Diffusion and permeation in heterogeneous media*. New York/London: Academic Press; 1968 [chapter 6].
- [19] Süer MG, Baç N, Yilmaz L. *J Membr Sci* 1994;91:77–86.
- [20] Siegel RA, Cussler EL. *J Membr Sci* 2004;229:33–41.
- [21] Nuxoll EE, Siegel RA, Cussler EL. *J Membr Sci* 2005;252:29–36.
- [22] Beaucage G, Schaefer DW. *J Non-Cryst Solids* 1994;58:1551–60.
- [23] Tanaka K, Kita H, Okano M, Okamoto K. *Polymer* 1992;33:585.
- [24] Freeman B, Pinnau I. *Polymer membranes for gas and vapor separation chemistry and materials science*. National Meeting of American Chemical Society, 1997, Las Vegas, Nevada ACS Symposium series 733, 149. New York: Oxford University Press; 1999 p. 115–126.
- [25] Duval JM, Folkers B, Mulder MHV, Desgrandchamps G, Smolders CA. *J Membr Sci* 1993;80:189–98.